Full-f gyrokinetic simulation including kinetic electrons

Y. Idomura[1,2], Y. Asahi[1], N. Hayashi[2] and H. Urano[2]

[1]Japan Atomic Energy Agency, Kashiwa, Japan
[2]National Institutes for Quantum and Radiological Science and Technology, Naka, Japan

Corresponding Author: idomura.yasuhiro@jaea.go.jp

Abstract:
A new hybrid kinetic electron model is developed for electrostatic full-f gyrokinetic simulations. The model is verified by computing the neoclassical transport and the linear ion temperature gradient driven trapped electron mode (ITG-TEM) stability. Impacts of kinetic electrons on the ITG turbulence are investigated, and a new saturation mechanism due to corrugated density profiles, which are generated by passing electrons transport, and new contributions from the field stress and the ion radial current to the toroidal angular momentum balance are found. Rotation changes and density peaking in the electron heating modulation experiment are qualitatively reproduced by a long time scale full-f ITG-TEM simulation over ~ 20 ms, in which electron heating modulation is applied. The mechanism of the rotation changes are explained by the ion radial current, which is reversed between ITG and TEM phases.

1 Introduction

Full-f gyrokinetic simulations disclosed rich physics such as self-organized critical phenomena in avalanche-like non-local transport [1] and interaction between turbulent and neoclassical transport channels [2], and validation studies on transport scalings with respect to the plasma size and the heating power [3] successfully recovered qualitative features of experimental transport scalings. Although capabilities of full-f gyrokinetic simulations have been greatly expanded, their electron models were limited to adiabatic electrons. This limitation prohibited us to address particle transport and electron heat transport, which are of critical importance in burning plasmas in ITER. In addition, recent electron heating modulation experiments [4, 5] suggest that transition of turbulence drive from ITG to TEM may play a critical role also in momentum transport. In order to resolve this limitation, in this work, we develop a new kinetic electron model for electrostatic full-f ITG-TEM simulations. In Sec.2, the model is described, and is verified by computing the neoclassical transport and the linear ITG-TEM. In Sec.3, impacts of kinetic electrons on the ITG turbulence are investigated, and finally, in Sec.4, rotation changes and density peaking observed in the electron heating modulation experiment [5] are examined in a long time scale full-f ITG-TEM turbulence simulation.

2 Hybrid kinetic electron model

GT5D solves a full-f gyrokinetic model with hybrid kinetic electrons [6], which consists of the full-f gyrokinetic equation in the gyro-center coordinates $\mathbf{Z} = (t; \mathbf{R}, v_\parallel, \mu, \alpha)$,

$$\frac{\partial \mathcal{J}_s f_s}{\partial t} + \nabla \cdot (\mathcal{J}_s \dot{\mathbf{R}} f_s) + \frac{\partial}{\partial v_\parallel}(\mathcal{J}_s \dot{v}_\parallel f_s) = \mathcal{J}_s \sum_{s'} C(f_s, f_{s'}) + \mathcal{J}_s S_{src,s}, \tag{1}$$

$$\dot{\mathbf{R}} = v_\parallel \mathbf{b} + \frac{c}{q_s B_\parallel^*} \mathbf{b} \times \left(q_s \nabla \langle \phi \rangle_\alpha + m_s v_\parallel^2 \mathbf{b} \cdot \nabla \mathbf{b} + \mu \nabla B \right), \tag{2}$$

$$\dot{v_\parallel} = -\frac{\mathbf{B}^*}{m_s B_\parallel^*} \cdot \left(q_s \nabla \langle \phi \rangle_\alpha + \mu \nabla B \right). \tag{3}$$

Here, f_s denotes the guiding-center distribution function, $\mathbf{R}$ is the position of the guiding center, $\mathbf{v}$ is the velocity of the guiding center, $v_\parallel = \mathbf{b} \cdot \mathbf{v}$ and $v_\perp = |\mathbf{b} \times \mathbf{v}|$ are the velocities in the parallel and perpendicular direction to the magnetic field, $\mu = m_s v_\perp^2 / 2B$ is the magnetic moment, α is the gyro-phase angle, $\mathbf{B} = B\mathbf{b}$ is the magnetic field, $\mathbf{b}$ is the unit vector in the parallel direction, m_s and q_s are the mass and charge of the particle species s, respectively, c is the velocity of light, $\Omega_s = q_s B / m_s c$ is the cyclotron frequency, $B_\parallel^* = \mathbf{b} \cdot \mathbf{B}^*$ is a parallel component of $\mathbf{B}^* = \mathbf{B} + (B v_\parallel / \Omega_s) \nabla \times \mathbf{b}$, ϕ is the electrostatic potential of turbulent fields, the gyro-averaging operator is defined as $\langle \cdot \rangle_\alpha \equiv \oint \cdot d\alpha / 2\pi$, $\mathcal{J}_s = m_s^2 B_\parallel^*$ is the Jacobian of the gyro-center coordinates, $C(f_s, f_{s'})$ is the multi-species linear Fokker-Planck collision operator, $S_{src,s}$ is a source term. Radial electric fields and turbulent fluctuations are respectively determined by non-axisymmetric and axisymmetric parts of the gyrokinetic Poisson equation,

$$\begin{aligned} &-\nabla_\perp \cdot \frac{\rho_{ti}^2}{\lambda_{Di}^2} \nabla_\perp \phi_{n \neq 0} + \frac{\alpha_p}{\lambda_{De}^2} \phi_{n \neq 0} \\ &= 4\pi \left[q_i \int f_{i,n\neq 0} \delta([\mathbf{R} + \rho] - \mathbf{x}) d^6 Z + q_e \int f_{e,t,n\neq 0} \delta([\mathbf{R} + \rho] - \mathbf{x}) d^6 Z \right], \end{aligned} \tag{4}$$

$$-\nabla_\perp \cdot \frac{\rho_{ti}^2}{\lambda_{Di}^2} \nabla_\perp \phi_{n=0} = 4\pi \sum_{s=i,e} q_s \int f_{s,n=0} \delta([\mathbf{R} + \rho] - \mathbf{x}) d^6 Z, \tag{5}$$

where n is the toroidal mode number, $\mathbf{R} + \rho$ is the particle position, $\rho = \mathbf{b} \times \mathbf{v} / \Omega_s$ is the Larmor radius, $\rho_{ts} = v_{ts} / \Omega_s$ is the Larmor radius evaluated with the thermal velocity $v_{ts} = (T_s / m_s)^{1/2}$, $\lambda_{Ds} = (T_s / 4\pi n_s q_s^2)^{1/2}$ is the Debye length, $f_{e,t}$ is a trapped part of the electron distribution function, and α_p is the flux-surface averaged fraction of passing electrons. The above model is equivalent to a multi-species gyrokinetic model, except for the second term in Eq.(4), in which passing electrons responses to turbulent fluctuations are assumed to be adiabatic. This approximation eliminates the so-called ω_H mode or the electrostatic limit of kinetic Alfven wave, which has very high frequency $\omega_H \sim \Omega_i$. Although such high frequency modes are unphysical from the viewpoint of the gyrokinetic ordering, it has been a bottleneck in long time scale gyrokinetic simulations. Although the conventional trapped electron models used this approximation also for Eqs.(1) and (5),

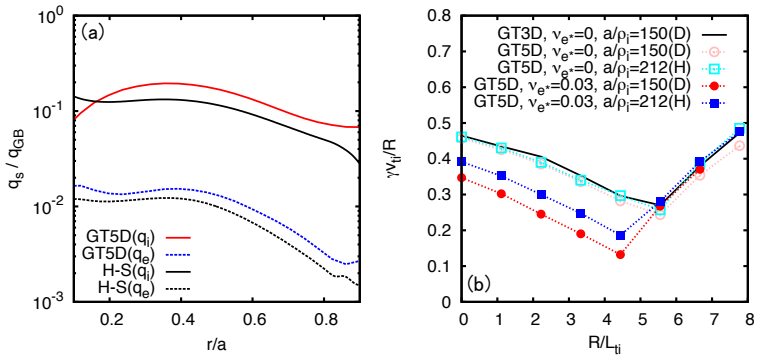

FIG. 1: (a) neoclassical ion and electron heat fluxes computed using GT5D and Hirshman-Sigmar 's moment approach (H-S) [7]. (b) linear ITG-TEM calculations for the former benchmark case [8] (GT3D). Also shown are comparisons of the ITG-TEM in deuterium and hydrogen plasmas, which show an isotope effect on the collisional stabilization of the TEM at the same electron collisionality ν_{*e}.

our model keeps them intact. This treatment is important for describing the neoclassical transport, the ambipolar condition, particle (de-)trapping processes, and passing electrons transport. The model is verified by computing the ion and electron neoclassical transport (see Fig.1(a)), zonal flow damping, and the linear ITG-TEM stability (see Fig.1(b)). In the linear ITG-TEM calculations, it is found that the isotope effect appears through the collisional stabilization of the TEM, which is characterized by the ratio of the electron collision frequency ν_e to the transit frequency of bulk ions $v_{ti,H}/R$ or $v_{ti,D}/R$.

3 Impact of kinetic electrons on turbulent transport

In this section, we show impacts of kinetic electrons on turbulent transport by comparing ITG turbulence simulations with adiabatic electrons and with kinetic electrons. In this work, we consider deuterium plasmas in a circular concentric tokamak configuration with $R/a = 2.79$, $a/\rho_{ti} = 150$, and $q(r) = 0.85 + 2.18(r/a)^2$, which has the Cyclone like parameters [9] at $r_s = 0.5a$: $\epsilon = r_s/R \sim 0.18$, $q(r_s) \sim 1.4$, $\hat{s}(r_s) = [(r/q)dq/dr]_{r=r_s} \sim 0.78$, $n_e \sim 4.6 \times 10^{19}\mathrm{m}^{-3}$, $R/L_n = 2.22$, $T_e \sim T_i \sim 2\mathrm{keV}$, $R/L_{te} = R/L_{ti} = 6.92$. Here, R is the major radius, a is the minor radius, r is the radial coordinate, q is the safety factor, n_e is the electron density, T_e and T_i are the electron and ion temperature, L_n, L_{te}, and L_{ti} are the corresponding scale lengths, and the above parameters lead to the normalized collisionality of $\nu_{*e} \sim 0.034$ and $\nu_{*i} \sim 0.024$. We use the hybrid electron model with the mass ratio of $m_i/m_e = 100$. The initial condition is given by a local Maxwellian distribution f_{s0} without parallel flows, $U_{||} = 0$. A source term with on-axis heating $(P_{in,i}, P_{in,e})$ and without particle and momentum input is imposed for $r = 0 \sim 0.4a$, while a Krook type sink operator is given for $r > 0.95a$ to impose a L-mode like fixed boundary condition with $n_e \sim 4 \times 10^{19}\mathrm{m}^{-3}$, $U_{||} = 0$, and $T_e = T_i \sim 1\mathrm{keV}$. From convergence tests in Ref. [6], numerical parameters are chosen as $(N_R, N_\zeta, N_Z, N_{v||}, N_\mu) = (160, 32, 160, 96, 20)$

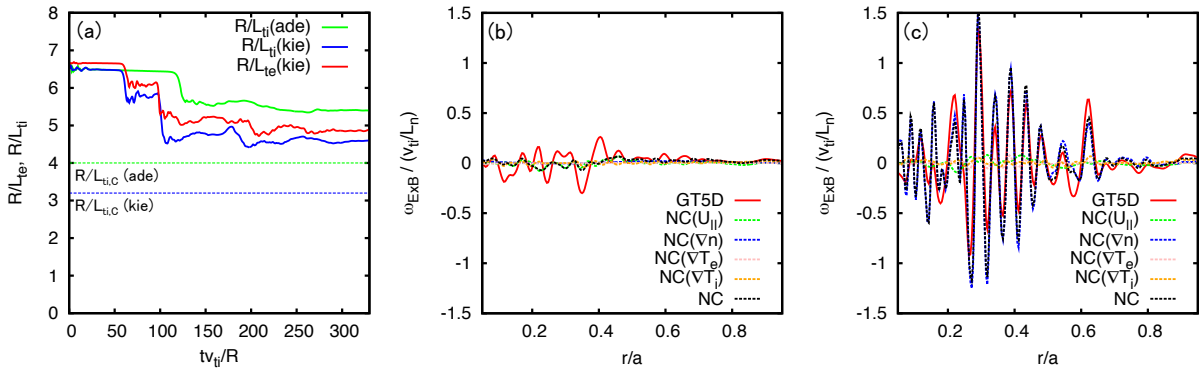

FIG. 2: (a) the time histories of $R/L_{ti}, R/L_{te}$ ($r/a = 0.4 \sim 0.6$) in decaying ITG turbulence. The linear critical temperature gradients are given at $R/L_{ti} = 4$ and $R/L_{ti} = R/L_{te} = 3.2$ for adiabatic and kinetic electrons, respectively. $E \times B$ shearing rates $\omega_{E\times B}$ in the final steady states are shown for the cases with (b) adiabatic and (c) kinetic electrons. Also shown are $\omega_{E\times B}$ estimated from the radial force balance relation (NC), and contributions from each term in it.

with 1/6 wedge torus model ($n = 0, 6, \cdots, 48$ or $k_\theta(r_s)\rho_{ti} = 0 \sim 0.9$), and $\Delta_t = 2\Omega_i^{-1}$.

Firstly, we compare nonlinear critical temperature gradients in decaying ITG turbulence simulations ($P_{in,i} = P_{in,e} = 0$). In decaying turbulence simulations, the ITG mode is excited from the linearly unstable initial condition, and the temperature profile is relaxed towards a nonlinear critical gradient, where turbulent transport is quenched. In contrast to the adiabatic electron case, where electron transport is neglected, the kinetic electron case shows significant electron transport even in the ITG turbulence. Since the magnetic drift gives opposite toroidal resonance conditions between ions and electrons, this electron transport is attributed to slab like resonance of passing electrons. In Fig.2(a), the resulting temperature relaxation occurs both for ions and electrons, and the final R/L_{ti} is lower in the kinetic electron case. In both cases, the nonlinear critical temperature gradients exhibit significant upshift from the linear ones. In the adiabatic electron case, this phenomenon is well known as the so-called Dimits shift [9], where the ITG mode is suppressed by turbulence driven zonal flows. However, in the kinetic electron case, the saturation mechanism is different. Figures 2(b) and 2(c) shows the $E \times B$ shearing rates $\omega_{E\times B}$ observed in the final steady states. In the adiabatic electron case, $\omega_{E\times B}$ ($\sim \gamma$) is produced in the plasma core, and its radial profile is largely deviated from an estimation with the radial force balance relation with neoclassical viscosity [7]. Therefore, $\omega_{E\times B}$ is mainly from turbulence driven (residual) zonal flows. On the other hand, in the kinetic electron case, $\omega_{E\times B}$ ($\gg \gamma$) is almost determined by the radial force balance relation. Here, the dominant contribution comes from corrugated density profiles, which are generated by passing electrons transport localized near mode rational surfaces [10]. This kind of coupling between particle and heat transport channels is a new turbulence saturation mechanism induced by kinetic electrons.

Another remarkable feature is that the direction of parallel flows are reversed from

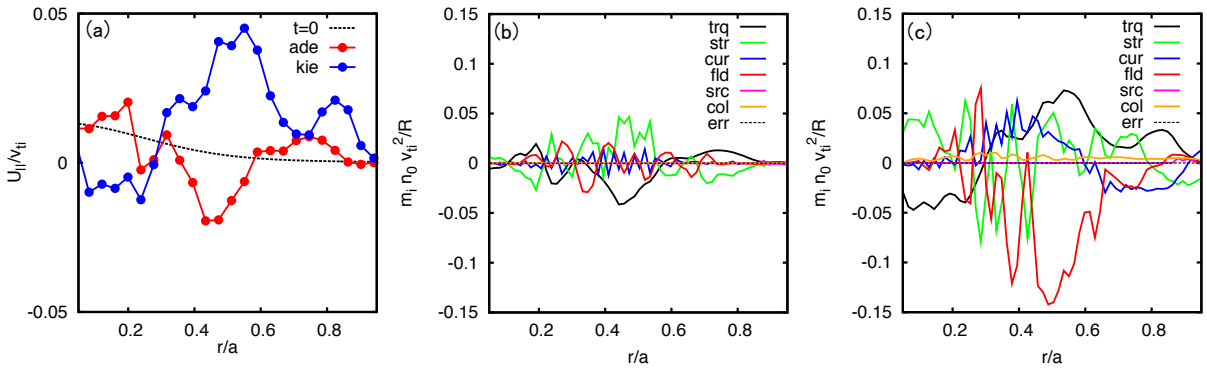

FIG. 3: (a) parallel flow profiles observed at $tv_{ti}/R \sim 330$ in fixed-flux ITG turbulence simulations. The toroidal angular momentum balance during the initial flow generation phase ($tv_{ti}/R = 50 \sim 330$) is plotted for the cases with (a) adiabatic and (b) kinetic electrons, respectively. Radial profiles of the torque (trq), the turbulent and neoclassical stress (str), the radial ion current (cur), the field stress (fld), the source term (src), and the collision term (col) in Eq.(6) are plotted.

the adiabatic electron case. Figure 3(a) shows parallel flow profiles observed in fixed-flux ITG turbulence simulations ($P_{in,i}$=4MW,$P_{in,e}$=0). Since the present simulations do not have momentum input in the plasma core, this difference is determined by turbulent momentum transport. In order to understand the flow generation process, we examine the ion component of the toroidal angular momentum balance [6],

$$\left\langle \frac{\partial m_i v_\parallel b_\varphi f_i}{\partial t} \right\rangle_{df} + \left\langle \frac{1}{\mathcal{J}} \frac{\partial}{\partial \mathbf{R}} \cdot \left(\mathcal{J} \dot{\mathbf{R}} m_i v_\parallel b_\varphi f_i \right) \right\rangle_{df} + \left\langle q_i f_i \frac{\partial \langle \phi \rangle_\alpha}{\partial \varphi} \right\rangle_{df} - \left\langle \frac{q_i}{c} f_i \dot{\mathbf{R}} \cdot \nabla \psi \right\rangle_{df}$$
$$- \left\langle m_i v_\parallel b_\varphi S_{src,s} \right\rangle_{df} - \left\langle m_i v_\parallel b_\varphi \sum_{s'} C(f_i, f_{s'}) \right\rangle_{df} = 0, \quad (6)$$

where b_φ is the covariant toroidal component of $\mathbf{b}$ and $\langle A \rangle_{df} = \langle \int A \delta(\mathbf{R} - \mathbf{x}) d^6 Z \rangle_f$ is the flux-surface average moment operator. Figures 3(b) and 3(c) show the time average of Eq.(6) over the initial flow generation phase. Compared with the adiabatic electron case, where the main contribution comes from the E_r shear stress [2], the kinetic electron case is characterized by a large contribution from the field stress $\langle q_i f_i \partial_\varphi \langle \phi \rangle_\alpha \rangle_{df}$, which is interpreted as the off-diagonal component of the electric part of the Maxwell stress tensor [11]. This effect is determined by the phase relation between the perturbed non-axisymmetric ion distribution δf_i and the toroidal electric field $\partial_\varphi \langle \phi \rangle_\alpha$. In the adiabatic electron model with $\delta n_e \propto \phi$, the phase difference is close to $\sim \pi/2$ and the field stress is not important. However, in the presence of trapped electrons, the phase difference is deviated from $\pi/2$, and the field stress is significantly enhanced. Another important difference is a finite contribution from the radial ion current induced by particle transport, which is neglected in the adiabatic electron case. In the next section, we examine the relevance of these new effects due to kinetic electrons in long time scale ITG-TEM turbulence simulations.

4 Electron heating modulation numerical experiment

In this section, we show a validation study on electron heating modulation experiments. Rotation changes induced by electron cyclotron resonance heating (ECRH) were observed in recent tokamak experiments [5, 4], and have attracted attention as new means to control plasma rotation without momentum input, because the external momentum input is expected to be small in ITER. In such ECRH modulation experiments, the electron temperature and its gradient are promptly increased by applying ECRH, and after the development of the electron temperature, plasma rotation is changed in the counter-current direction, and density peaking is often observed simultaneously in the time scale of several tens of ms [5]. These transient changes have been considered to be attributed to transition of turbulence drive from ITG to TEM, and the density peaking was well explained by flux-tube gyrokinetic calculations [12]. However, the momentum transport has been still an open issue. To address this issue, we apply electron heating modulation to a long time scale full-f ITG-TEM turbulence simulation over $\sim$ 20ms.

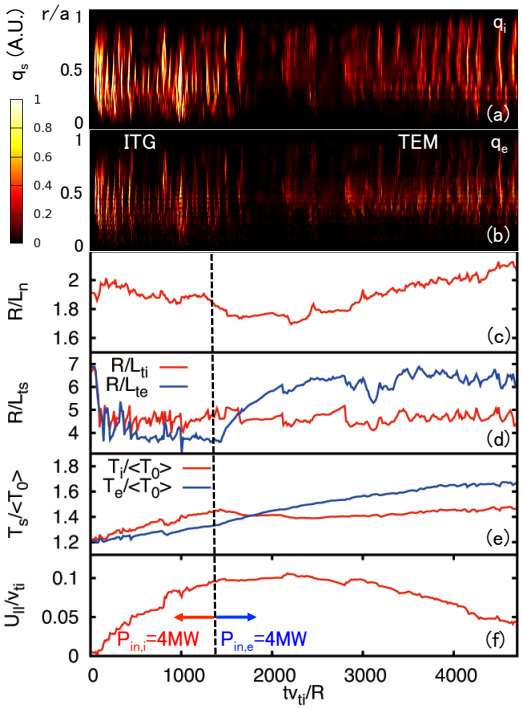

FIG. 4: An electron heating modulation numerical experiment. (a) and (b) show time and radial evolutions of ion and electron heat fluxes, respectively. The time histories of (a) R/L_n, (b) $R/L_{ti}, R/L_{te}$, (c) T_i, T_e, and (d) $U_{||}$ are observed at $r \sim 0.5a$.

In Fig.4, the ITG turbulence simulation with ion heating ($P_{in.i}$=4MW,$P_{in,e}$=0) is continued until the quasi-steady state with the co-current intrinsic rotation is established, and then, at $tv_{ti}/R \sim 1400$, the heating condition is switched to electron heating ($P_{in.i}$=0,$P_{in,e}$=4MW). By applying the electron heating, R/L_{te} and T_e/T_i are quickly increased ((d),(e)), and the onset of TEM occurs around $tv_{ti}/R \sim 2800$. Both in the ITG and TEM phases, ion and electron heat fluxes show similar avalanche like nonlocal transport ((a),(b)). During the TEM phase, R/L_n is gradually increased, and parallel flows are changed in the counter-current direction ((c),(f)). These observations are qualitatively consistent with the experiment [5], and shows the validity of the new hybrid kinetic electron model.

In order to understand the mechanism of the rotation changes in Fig.5(a), the ion toroidal angular momentum balance is studied both in the ITG and TEM phases in Figs.5(b) and 5(c). Unlike the initial saturation phase of the ITG turbulence, the role of the field stress is changed in the quasi-steady turbulence, and it tends to cancel the turbulent and neoclassical stress (the second term in Eq.(6)) both in the ITG and TEM phases. This cancellation is qualitatively different from the cancellation between the turbulent stress and the neoclassical stress in the quasi-steady ITG turbulence with adiabatic

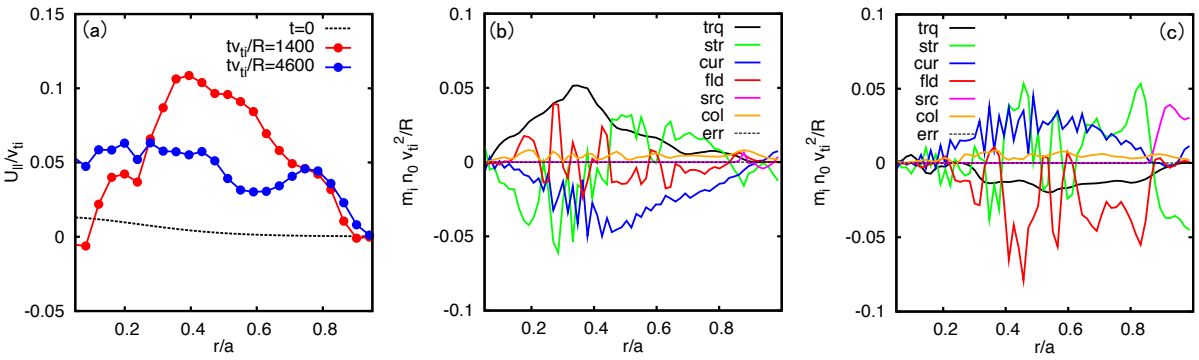

FIG. 5: (a) parallel flow profiles at $tv_{ti}/R = 1400$ and $tv_{ti}/R = 4600$ in the electron heating modulation numerical experiment. (b) and (c) show the ion toroidal angular momentum balance in the ITG phase ($tv_{ti}/R = 400 \sim 1400$) and in the TEM phase ($tv_{ti}/R = 3600 \sim 4600$), respectively.

electrons, where the field term stress is small [2]. As a result, the remaining contribution to the torque comes from the ion radial current, which is reversed by particle pinch in the TEM phase. It is noted that since the ambipolar condition is satisfied between ions and electrons, the similar electron radial current exists in the electron part of the toroidal angular momentum balance. However, the electron radial current is almost cancelled by the electron field stress, and the net torque is determined only by ions. These results suggest a new momentum transport mechanism induced by coupling between particle and momentum transport channels.

5 Summary

In this work, we developed a new hybrid kinetic electron model, which enables long time scale full-f ITG-TEM simulations. The model was verified by computing the neoclassical transport and the linear ITG-TEM stability. By using the model, we studied impacts of kinetic electrons on the ITG turbulence, and clarified the following two important effects. One is a new saturation mechanism due to corrugated density profiles and the resulting fine E_r, which are generated by passing electrons transport localized near mode rational surfaces. The other is new contributions from the field stress and the ion radial current to the toroidal angular momentum balance. These new effects suggest an importance of coupling between multiple transport channels such as indirect suppression of heat transport by particle transport and rotation drive by particle transport. Based on the above physics understanding, we conducted a long time scale ITG-TEM turbulence simulations for $\sim$ 20 ms, in which electron heating modulation was applied as in the ECRH modulation experiment. The numerical experiment successfully reproduced rotation changes and density peaking induced by transition of turbulence drive from ITG to TEM, and the validity of the new model was demonstrated. In the numerical experiment, it was

found that the turbulent and neoclassical stress is cancelled by the field stress, and the remaining contribution comes from the radial ion current, which is reversed by particle pinch in the TEM phase.

The computation in this work was performed on the Helios at the IFERC, the FX100 at the Nagoya Univ., the Plasma Simulator at the NIFS, and the K-computer (hp160208) at the Riken. This work is supported by the MEXT, Grant for HPCI Strategic Program Field No.4: Next-Generation Industrial Innovations, Grant for Post-K priority issue No.6: Development of Innovative Clean Energy, and Grant No. 22686086.

References

[1] Y. Idomura, et al. Study of ion turbulent transport and profile formations using global gyrokinetic full-f vlasov simulation. *Nuclear Fusion*, Vol. 49, p. 065029, 2009.

[2] Y. Idomura. Full-f gyrokinetic simulation over a confinement time. *Physics of Plasmas*, Vol. 21, p. 022517, 2014.

[3] Y. Idomura and M. Nakata. Plasma size and power scaling of ion temperature gradient driven turbulence. *Physics of Plasmas*, Vol. 21, p. 020706, 2014.

[4] M. Yoshida, et al. Rotation drive and momentum transport with electron cyclotron heating in tokamak plasmas. *Physical Review Letters*, Vol. 103, p. 065003, 2009.

[5] R. M. McDermott, et al. Effect of ECRH on toroidal rotation in asdex upgrade h-mode discharges. *Plasma Physics and Controlled Fusion*, Vol. 53, p. 035007, 2011.

[6] Y. Idomura. A new hybrid kinetic electron model for full-f gyrokinetic simulations. *Journal of Computational Physics*, Vol. 313, pp. 511–531, 2016.

[7] S. P. Hirshman and D. J. Sigmar. Neoclassical transport of impurities in tokamak plasmas. *Nuclear Fusion*, Vol. 21, p. 1079, 1981.

[8] G. Rewoldt, Z. Lin, and Y. Idomura. Linear comparison of gyrokinetic codes with trapped electrons. *Computer Physics Communications*, Vol. 177, p. 775, 2007.

[9] A. M. Dimits, et al. Comparisons and physics basis of tokamak transport models and turbulence simulations. *Physics of Plasmas*, Vol. 7, pp. 969–983, 2000.

[10] Y. Idomura. Saturation mechanism of decaying ion temperature gradient driven turbulence with kinetic electrons. *Plasma and Fusion Research*, Vol. 11, p. 2403006, 2016.

[11] J. Abiteboul, et al. Conservation equations and calculation of mean flows in gyrokinetics. *Physics of Plasmas*, Vol. 18, p. 082503, 2011.

[12] C. Angioni. Gyrokinetic modelling of electron and boron density profiles of h-mode plasmas in asdex upgrade. *Nuclear Fusion*, Vol. 51, p. 023006, 2011.